JOURNAL OF PROPULSION AND POWER
Vol. 15, No. 6, November–December 1999

Computed Flammability Limits of Opposed-Jet $H_2/O_2/CO_2$ Diffusion Flames at Low Pressure

Hsin-Yi Shih,* Hasan Bedir,† James S. T'ien,‡ and Chih-Jen Sung§
Case Western Reserve University, Cleveland, Ohio 44106

A narrowband radiation model is coupled to the OPPDIF program to enable the study of one-dimensional hydrogen–oxygen diffusion flame over the entire range of flammable stretch rates. The flame characteristics and the extinction limits at a low pressure of 1.013 kPa are sought, with the amount of carbon dioxide dilution level and stretch rate as parameters. The conditions studied are particularly relevant to Mars exploration. In addition, a flammability map is presented using these two parameters as coordinates. Both the high-stretch blowoff and the low-stretch quenching limits are found. The existence of an absolute carbon dioxide dilution limit, above which the diffusion flame is not possible, is demonstrated. Low-stretch diffusion flames at low pressures are unusually thick, with flame temperatures substantially below those of the adiabatic flames. This large temperature drop results from the combined effect of flame radiation and limited gas residence time in the flame, and may be particular to the hydrogen–oxygen chemical kinetics. One of the novel features of the application of the narrowband radiation model is the inclusion of Doppler broadening, which is shown to be important in low-pressure flames.

Nomenclature

a = stretch rate (velocity gradient on the fuel side)
C_p = constant-pressure specific heat
D_{kj} = multicomponent diffusion coefficient
D^T = thermal diffusion coefficient
h = enthalpy
I = radiative intensity
P = pressure
pl = pressure path length
q_r = radiative heat flux
s, s' = direction along a ray
T = temperature
U = nondimensional radial velocity
V = axial mass flux
v = diffusion velocity
W = molecular weight
X = mole fraction
Y = mass fraction
y = axial direction
β = mean line width to spacing ratio
γ = line half-width
δ = line spacing parameter
κ = mean absorption coefficient
λ = heat conduction coefficient
μ = viscosity or direction cosine
ν = wave number
ρ = density
τ = transmittance
ω = production rate

Subscripts

b = blackbody
C = collision
D = Doppler
k = species index
$+\infty$ = oxygen side
$-\infty$ = fuel side

Received 11 August 1998; revision received 12 January 1999; accepted for publication 12 January 1999.

The senior author (JST) would like to dedicate this paper in the memory of Martin Summerfield, who introduced the field of propulsion and combustion to him. His four years as a graduate student at Princeton University under the coadvisorship of William A. Sirignano and Martin Summerfield are among the most cherished of his life.

*Graduate Student, Department of Mechanical and Aerospace Engineering.

†Graduate Student, Department of Mechanical and Aerospace Engineering; currently Assistant Professor, Department of Mechanical and Aerospace Engineering, Bogazici University, Bebek, 80815, Istanbul, Turkey.

‡Professor, Department of Mechanical and Aerospace Engineering, and Senior Scientist, National Center for Microgravity Research on Fluids and Combustion. Associate Fellow AIAA.

§Assistant Professor, Department of Mechanical and Aerospace Engineering, and Staff Scientist, National Center for Microgravity Research on Fluids and Combustion. Senior Member AIAA.

Introduction

COMBUSTION of hydrogen with oxygen has been the research topic in numerous studies both because of its importance as a practical fuel in propulsion systems and because it is an important intermediate in the burning of hydrocarbons. Fundamental studies of hydrogen–oxygen diffusion flame structure and extinction limits have been carried out both experimentally and theoretically using opposed-jet (counterflow) geometry. In this configuration, an approximately one-dimensional laminar flame can be achieved, which simplifies the theoretical description. The literature on counterflow hydrogen–oxygen diffusion flames is abundant. A recent paper[1] has summarized many experimental results, and comparisons have been made with the available theoretical calculations. It contains most of the relevant background and is not repeated here. In these previous studies, the emphasis on the extinction phenomena was on the blowoff limits, that is, extinction due to insufficient gas residence time at large stretch rates. The blowoff limit is obviously important in high-speed flow and in high-intensity turbulent flames containing flamelets. On the other hand, diffusion-flame extinction due to heat losses (e.g., radiation) is a relatively newly studied phenomenon that occurs in weak flames. The recent activity in microgravity combustion has been instrumental in incorporating radiation into the flame models.[2,3]

To achieve a radiatively quenched limit, one generally needs to slow convection in a flame. One such flame with simple one-dimensional configuration is the opposed-jet diffusion flame at low stretch rates.[4–10] These studies show that the extinction boundary consists of two branches: the high-stretch blowoff branch due to insufficient residence time and the low-stretch quenched branch due to radiative loss. The merging point of these two branches defines a

fundamental limit beyond which diffusion flames cannot exist at any stretch rate. For example, if the extinction boundary is plotted using stretch rate and ambient oxygen percentage as coordinates, this limit is the lowest oxygen percentage to sustain a diffusion flame. The fundamental limit is a conservative index from the point of view of fire safety because, beyond it, the flame cannot exist regardless of the dynamic condition (e.g., stretch rate). These previous studies also show that the fundamental limit occurs at a relatively low stretch rate, which is generally outside the range of most laboratory experiments. From a theoretical point of view, the merging point of the two extinction branches is the result of the combined influence of stretch and radiation. Therefore, an accurate computation of this limit condition requires accurate transport, kinetic, and radiation treatments and the inclusion of low-stretch regime.

Depending on the detailed treatment of chemical kinetics and radiation, past computational works of low-stretch diffusion flames can be divided into several groups: 1) global kinetics with gray surface radiative loss [for solid polymethylmethacrylate (PMMA) fuel],[4] 2) narrowband gas radiation model for gaseous species with global kinetics (for solid PMMA fuel),[5,6] and 3) detailed kinetics with optically thin flame radiation for methane.[7,8] Although all of these works appear to give the correct extinction trend and hence the essential physics, quantitatively much can be improved. It is known that global kinetics lack the accuracy to make quantitative prediction (unfortunately, for most complex solid fuels, detailed gas-phase kinetics are not completely understood). On the other hand, the use of an optically thin radiation model has been shown to overpredict flame radiative loss.[9,11] Self-absorption from gaseous species renders the flame nonoptically thin. It appears that a combination of detailed kinetics with a narrowband radiation model provides the best match at this time.

The first work using this combination is that by Daguse et al.[9] They studied nitrogen-diluted hydrogen diffusion flame with air at 1 atm pressure. Both high-stretch and low-stretch extinction limits are determined in the computation. Results using this combination in another flame geometry, that is, flame ball in microgravity, have been computed.[12] The present work studies theoretically the hydrogen–oxygen diffusion flame, but with carbon dioxide as a diluent and at a low pressure. This choice is based on the following objectives: First, carbon dioxide is a strong radiation-participating gas. By varying the amount of carbon dioxide, the effect of flame radiation can be studied more readily. Note that carbon dioxide has been used as a practical flame-extinguishing agent. Second, there is interest in the fire safety aspect of hydrogen as a feedstock of methane production in the proposed in-situ resource utilization scheme in the future exploration of Mars.[13] Carbon dioxide is the main component of the Martian atmosphere, and the average atmospheric pressure on Mars is about 0.01 of Earth's atmospheric pressure. The chosen diluent in this theoretical study is therefore carbon dioxide and the pressure is 1.013 kPa. As will be seen later, the combination of low pressure and low stretch results in an unusually thick diffusion flame. The low-pressure condition also requires a special treatment of the radiation model.

Mathematical Formulation

The flame configuration considered is a counterflow, axisymmetric laminar diffusion flame, stabilized near the stagnation plane of two opposing jet flows. Two equivalent formulations of the problem exist in the literature[14]: one specifying the flame stretch rate and the other the jet exit velocity and nozzle separation distance. The constant stretch rate formulation is utilized in this paper. If one assumes that the density ρ, temperature T, mass fractions Y_k, nondimensional radial velocity U, and axial mass flux V are functions only of the axial direction y, then the resulting equations are[15]

Continuity:

$$\frac{\mathrm{d}V}{\mathrm{d}y} + 2\rho a U = 0 \tag{1}$$

Momentum:

$$V\frac{\mathrm{d}U}{\mathrm{d}y} - \frac{\mathrm{d}}{\mathrm{d}y}\left(\mu\frac{\mathrm{d}U}{\mathrm{d}y}\right) - a\left(\rho_\infty - \rho U^2\right) = 0 \tag{2}$$

Energy:

$$Vc_p\frac{\mathrm{d}T}{\mathrm{d}y} - \frac{\mathrm{d}}{\mathrm{d}y}\left(\lambda\frac{\mathrm{d}T}{\mathrm{d}y}\right) + \left(\sum_{k=1}^{K}\rho Y_k V_k c_{pk}\right)\frac{\mathrm{d}T}{\mathrm{d}y} + \sum_{k=1}^{K}\dot{\omega}_k h_k + \frac{\mathrm{d}q_r}{\mathrm{d}y} = 0 \tag{3}$$

Species:

$$V\frac{\mathrm{d}Y_k}{\mathrm{d}y} + \frac{\mathrm{d}}{\mathrm{d}y}(\rho Y_k V_k) - \dot{\omega}_k = 0, \qquad k = 1, \ldots, K \tag{4}$$

The equation of state is

$$\rho = (PW/RT) \tag{5}$$

where W is the mixture molecular weight given by

$$W = \left(\sum_{k=1}^{K}\frac{Y_k}{W_k}\right)^{-1} \tag{6}$$

The diffusion velocities are defined as

$$v_k = \frac{1}{X_k W}\sum_{j=1}^{K} W_j D_{kj}\frac{\mathrm{d}X_j}{\mathrm{d}y} - \frac{D_k^T}{\rho Y_k}\frac{1}{T}\frac{\mathrm{d}T}{\mathrm{d}y} \tag{7}$$

where D_{kj} is the multicomponent diffusion coefficient, D_k^T is the thermal diffusion coefficient, X_k is the mole fraction, and W_k is the molecular weight of kth species.

The boundary conditions for the preceding equations are

$$T(+\infty) = T_{+\infty} \tag{8}$$

$$T(-\infty) = T_{-\infty} \tag{9}$$

$$Y_k(+\infty) = Y_{k,+\infty}, \qquad k = 1, \ldots, K \tag{10}$$

$$Y_k(-\infty) = Y_{k,-\infty}, \qquad k = 1, \ldots, K \tag{11}$$

$$U(-\infty) = 1 \tag{12}$$

$$U(+\infty) = (\rho_{-\infty}/\rho_{+\infty})^{\frac{1}{2}} \tag{13}$$

$$V(y = 0) = 0 \tag{14}$$

Fuel and oxidizer jets are located at negative and positive infinity, respectively. The same mole fraction of CO_2 dilution at both the hydrogen and the oxygen sides is assumed. The inlet temperature of reactants is 300 K. Note that the quantity a in Eqs. (1) and (2) is the fuel-side stretch rate, consistent with the boundary conditions given in Eqs. (12) and (13). The stagnation point is at $y = 0$ as indicated in Eq. (14). The last term in the energy equation (3), $\mathrm{d}q_r/\mathrm{d}y$, represents the contribution from flame thermal radiation. The treatment of this term is given in the next section.

Narrowband Radiation Model

A comparison of different treatments for one-dimensional diffusion flames has been made in Ref. 11. Optically thin and gray models have been shown to be inadequate for quantitative predictions. In this work, a statistical narrowband model with the exponential tailed inverse line strength distribution is used to calculate the radiative properties of the participating gases assumed in the calculations (CO, CO_2, and H_2O). A particular feature of the present treatment is that, in the transmittance calculations, both the Doppler broadening

and the collision broadening are considered. For flames at normal Earth atmospheric conditions, the collision broadening is the most important broadening mechanism. The collision broadening is proportional to pressure and inversely proportional to the square root of the temperature. Doppler broadening, on the other hand, is not proportional to pressure. Therefore, at the low pressure (0.01 Earth atm) considered in this paper, the collision broadening is reduced and the importance of the Doppler broadening is increased, as will be shown in the following sections.

The transmittance τ of a homogeneous gas column with combined collision and Doppler broadening is given by Ref. 16:

$$\tau = \exp\left(-kpl\sqrt{1-\theta^{-\frac{1}{2}}}\right)^{\frac{1}{2}} \tag{15}$$

$$\theta = \left[1-(X_C/kpl)^2\right]^{-2} + \left[1-(X_D/kpl)^2\right]^{-2} - 1 \tag{16}$$

In these expressions, k is the mean absorption coefficient and pl is the pressure path length. X_C and X_D are the equivalent widths for collision and Doppler broadening, respectively.

The collision equivalent width X_C is given by

$$X_C = (\beta/\pi)\left(\sqrt{1+(2\pi kpl/\beta)}-1\right) \tag{17}$$

where $\beta = 2\pi\gamma_C/\delta$ is the mean linewidth to spacing ratio. The collision half-width expression γ_C and the line spacing parameter δ are taken from Soufiani and Taine.[17]

The Doppler equivalent width X_D is given by Ref. 16:

$$X_D = 1.7\gamma_D\left(\ell n\left\{1+[0.589(kpl/\gamma_D)]^2\right\}\right)^{\frac{1}{2}} \tag{18}$$

The Doppler half-width γ_D is calculated from the following expression[16]:

$$\gamma_D = 5.94\times10^{-6}\left(\nu/\sqrt{W}\right)\sqrt{T/273} \tag{19}$$

The preceding formulas are extended to the nonhomogeneous case with the use of the Curtis–Godson approximation.[18] With this approximation, the nonhomogeneous gas properties are obtained from the same expressions using equivalent parameters.

The radiative source term in Eq. (3) is given by the nongray radiative transport equation for an absorbing and emitting medium written in terms of the mean transmittance over a narrowband[19]:

$$\frac{\partial I_\nu(s,\Omega)}{\partial s} = \left.\frac{\partial\tau_\nu(s'\to s)}{\partial s'}\right|_{s'=s} I_{b\nu}(s) + I_{w\nu}(s_w,\Omega)\frac{\partial}{\partial s}\{\tau_\nu(s_w\to s)\} + \int_{s_w}^{s}\frac{\partial}{\partial s}\left[\frac{\partial\tau_\nu(s'\to s)}{\partial s'}\right] I_{b\nu}(s')\,\mathrm{d}s' \tag{20}$$

When the spectral intensity I_ν is calculated, the radiative source term is obtained from a double integration over the solid angle Ω and the wave number ν:

$$\frac{\mathrm{d}q_r}{\mathrm{d}y} = \frac{\mathrm{d}}{\mathrm{d}y}\sum_{\Delta\nu}\left[\int_{4\pi}\mu I_\nu(y,\Omega)\,\mathrm{d}\Omega\right]\Delta\nu \tag{21}$$

The constant-stretch opposed-jet diffusion flame equations (1–4) were solved coupled with the narrowband radiative transfer equation (20). The OPPDIF program by Lutz et al.[20] was modified and utilized in the solutions. First, this program was converted from the constant-velocity formulation to the constant-stretch formulation. Second, the statistical narrowband solver was coupled with the OPPDIF program. The nongray narrowband radiative transfer equation was solved with the S_8 discrete ordinates method. A 20-direction Gaussian quadrature set was used. The radiation participating gaseous species included are CO, CO_2, and H_2O; their narrowband radiative properties were taken from Ref. 17.

The solution of the governing equations (1–4) also requires the knowledge of transport coefficients (λ, μ) and the thermodynamic properties (c_p, c_{pk}, h_k). These data were determined using the CHEMKIN and TRANSPORT package.[21,22] The chemical production rates ω_k as functions of the state variables T, P, and Y_k have to be provided by the user. In this work, the detailed kinetics scheme of $CO/H_2/O_2$ flame was taken from Kim et al.[23] with 11 species and 30 reactions. Using this set of data, a comparison with existing results was made by performing a computation of pure hydrogen with air at standard atmospheric condition (300 K and 101.3 kPa) without radiation. The computed blowoff limit at an air-side stretch rate was found to be 9155 l/s. This is comparable to the values of 8140 l/s in Ref. 24 and 8060 l/s in Ref. 25, especially in view of the uncertainties in kinetics rate constants, thermodynamic/transport properties, and the transport descriptions. For instance, thermal diffusion is neglected in Ref. 24, but it is included in the present calculation. It is further noted that thermal diffusion tends to increase the blowoff extinction limit.

A grid independence check also has been performed. In the OPPDIF program, variable grid distribution is used and the grid sizes are adaptable. Grid sizes are controlled by specifying the acceptable first and second gradients in the solution. The difference between the present results and the ones with much more stringent gradient specifications is minimal. For example, the difference of the maximum temperatures in Fig. 4 is less than 4 K (out of 1230 K). So, the present results are essentially grid independent.

Results

Computations were performed using fuel-side stretch rate and molar percentage of CO_2 dilution (same on the fuel and the oxidizer sides) as parameters. Figure 1 shows the maximum flame temperatures as a function of stretch rates at 50% CO_2 dilution, with and without the consideration of flame radiation. The first observation is that all of the burning solutions in this figure are located in the low-stretch regime ($a < 40$ l/s). The second observation is that, with radiation, the flame temperature exhibits a peak at an intermediate stretch rate for a given CO_2 dilution. This result contrasts to the case without radiation, which shows a monotonic trend with respect to stretch rate. Compared with the computed values without radiation, this difference becomes larger as stretch rate is decreased. Clearly, the drop of flame temperature at the low stretch end is due to flame radiative loss. Therefore, the flame response to the right and the left of the intermediate stretch rate, where the flame temperature peaks, is dominated by flame stretch and flame radiation, respectively. Although this trend has been identified in previous works, the use of more accurate kinetic and radiative data

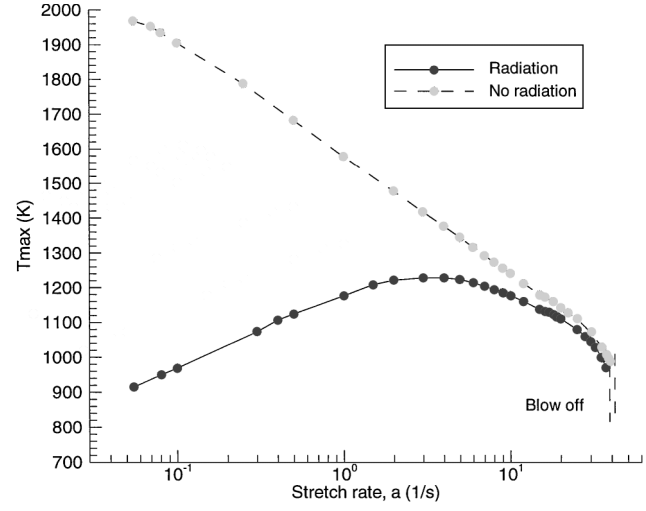

Fig. 1 Maximum temperature of H_2/O_2 diffusion flame as a function of stretch rate (fuel side) at a total pressure of 1.013 kPa and 50% CO_2 dilution (same on the fuel and the oxygen sides), with and without the consideration of flame radiation.

in this paper enables the quantitative difference to be assessed with more confidence. To further a discussion on the mechanisms of the flame temperature drop, the curve of 50% CO_2 without radiation is first examined. The computed adiabatic flame temperature for 50% CO_2 dilution is 1972 K. At the blowoff limit, the flame temperature is 989 K. This temperature is more than 900 K below the adiabatic value! The flame temperature increases with decreasing stretch rate, approaching the adiabatic limit only when $a < 0.1\ s^{-1}$. The fast kinetic approximation fails for $a > 0.1\ s^{-1}$, basically for the entire computed range of stretch rate shown in Fig. 1. For the no-radiation case, the temperature reduction is the result of insufficient gas residence time. Additional calculations using a residence-time-limited chemical system, namely a perfectly stirred reactor, have been carried out to further quantity the characteristic chemical reaction time. Results show that the critical residence time leading to the extinction of the homogeneous system is about 0.02 s with flame temperature of 1030 K, at a low pressure of 1.013 kPa. Such a kinetics limit is seen to compare quite well with the state at the blowoff limit, in terms of either extinction stretch rate or extinction temperature. Furthermore, the homogeneous calculations demonstrate that the system temperature is within 100 K of the adiabatic flame temperature when the residence time exceeds 10 s. This result is consistent with the results shown earlier that the nonradiation flame approaches the adiabatic limit only when the stretch rate is reduced below $0.1\ s^{-1}$. As for the curves with radiation in Fig. 1, the drop of flame temperature at low stretch is the result of increasing radiative loss. Compared with the computed values without radiation at 50% CO_2, this difference can grow to be very large as stretch rate is decreased.

The maximum flame temperatures of the radiating flames at different CO_2 dilution levels are shown in Fig. 2. For all the radiation cases shown in here, the flame temperatures are quite low. The computed adiabatic flame temperatures for 50, 60, 70, and 75% CO_2 are 1972, 1743, 1410, and 1224 K, respectively. The reason for the flame temperature being lower than the corresponding adiabatic flame temperature is because of the slow chemistry at low pressure, insufficient residence time, and radiative loss. As CO_2 dilution level is increased, the stretch rate at which the flame temperature peaks moves to a smaller value. As discussed earlier, the peak of flame temperature for a given CO_2 dilution can be used as an indicator of the relative importance of radiative loss vs flame stretch, which we illustrated later. The vertical dashed lines in Fig. 2 indicate the extinction limits. Although all of the blowoff limits are given, only the quenching limits at 70 and 75% CO_2 are shown. For the other cases, the quenching limits at lower stretch rates were not computed.

Note also in Figs. 1 and 2 that although the flame extinction temperature can be substantially below the corresponding adiabatic flame temperature, the extinction temperature is nearly independent of the adiabaticity of system, the extent of dilution, and the controlling extinction mechanisms (either stretch induced or radiation induced). In fact, the extinction temperature compares quite well with the crossover temperature, which is around 651 K at 1.013 kPa.[26] The crossover temperature is determined when the reaction rates of two competing H-O_2 steps are equal:

$$H + O_2 \rightarrow OH + O \tag{22}$$

$$H + O_2 + M \rightarrow HO_2 + M \tag{23}$$

Note that reaction (22) is a two-body, temperature-sensitive branching reaction, whereas reaction (23) is a three-body temperature-insensitive terminating reaction because the intermediate HO_2 is relatively inactive. Thus, increasing temperature facilitates reaction (22) and hence the overall reactivity, whereas increasing pressure facilitates the three-body reaction (23) over the two-body reaction (22) and hence retards the overall reactivity. This, therefore, explains the increase of the crossover temperature with increasing pressure. Because this limiting temperature represents the transition in dominance between chain-branching and chain-termination reactions, it is expected that abrupt extinction should occur whenever the flame temperature is reduced close to the crossover temperature. The remarkable agreement between the extinction and the crossover temperatures signifies the resilience of the hydrogen–oxygen flame to extinction.

The flammability map in Fig. 3 presents a more complete picture. First, without radiation, the extinction boundary is monotonic with respect to stretch rate. From the trend of the computed boundary, there is no apparent low-stretch limit; when the CO_2 dilution level is increased, the flame can still be made flammable at lower stretch rates. Furthermore, it is seen that the adiabatic system would cease to be flammable only when the CO_2 dilution is beyond 90% (obtained by extrapolating the stretch rate to zero). With radiation, low-stretch quench limits exist and the trend of the extinction boundary is altered. This behavior helps to define an absolute CO_2 dilution level above which flame cannot exist at any stretch rate. The existence and the determination of this dilution level can be important from the point view of fire safety. For the present diffusion flame at 1.013 kPa and an upstream temperature of 300 K, this dilution limit is 81% CO_2, equally from the fuel and the oxygen sides.

As seen in Fig. 2, the flame temperature curves relative to stretch rate exhibit a maximum for a given CO_2 percentage. The locus of this maximum flame temperature is plotted along with the extinction boundary in Fig. 3. In the region bounded by this locus and the blowoff boundary, flame behavior is dominated by flame stretch. On the other hand, in the region bounded by this locus and the quenching boundary, the flame behavior is dominated by radiation.

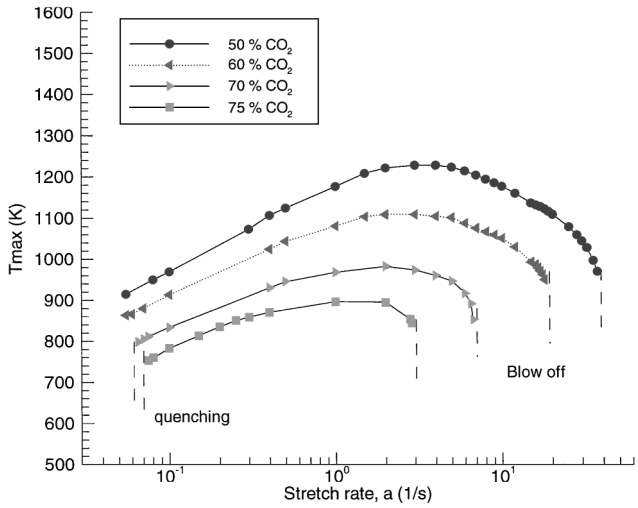

Fig. 2 Maximum flame temperature of H_2/O_2 diffusion flame with radiation as a function of stretch rate at different CO_2 dilution levels.

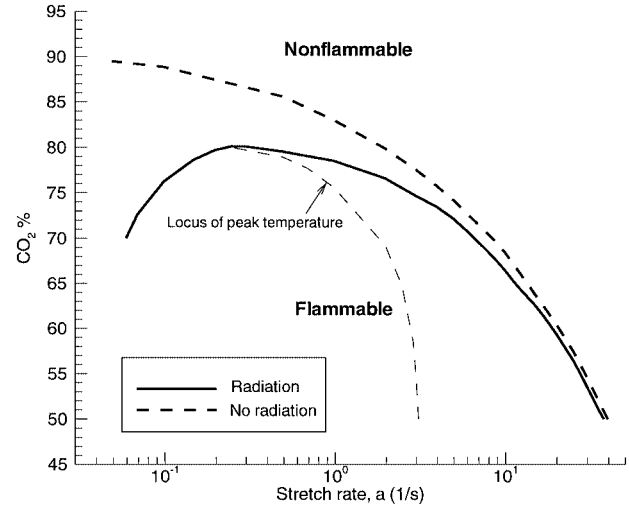

Fig. 3 Flammability boundary of $H_2/O_2/CO_2$ opposed-jet diffusion flame with and without consideration of flame radiation (total pressure = 1.013 kPa; upstream temperature = 300 K).

As mentioned earlier, the quenching limits for CO_2 less than 70% were not computed because they occur at very low stretch rates.

Flame Structure

The flame structure at a low stretch rate ($a = 3\ s^{-1}$, 50% CO_2) for cases with and without radiation are shown in Fig. 4. In this and the following figure, the distance (Y_s) is measured from the stagnation point. The flame is about 15 cm thick (measured at the intermediate temperature). In contrast, a PMMA solid diffusion flame at the same stretch rate was found to have a flame thickness of approximately 2 cm in experiments performed at 1 Earth atm pressure.[10] The unusual flame thickness in the present case is the combined result of low pressure (1% of Earth atm), high diffusivity of hydrogen, and low flame stretch. To be able to have a one-dimensional flame with this thickness experimentally, a special setup is required. This setup is discussed later.

The temperature peak is located 2 cm from the stagnation point on the oxygen side. The region with substantial overlap of H_2 and O_2 is of the order of 10 cm. Hydrogen peaks near the stagnation point on the fuel side of the flame, whereas O and OH are aligned closer to the temperature peak on the oxygen side away from the stagnation point. The concentrations of O and OH show substantial sensitivity to radiation treatments (through temperature difference in the two cases), whereas the H concentration is less sensitive.

Comparing the cases with and without radiation, the radiative flame temperature is about 200 K lower than that of the adiabatic value. In addition, the radiative flame is narrower in the high-temperature region. Longer tails are predicted on both the fuel and the oxygen sides because of the radiative absorption by CO_2 (the characteristic length for flame radiation is considerably longer than that for conduction or diffusion). Interestingly, the CO_2 profile has a peak and a valley and CO also exists in the flame. CO_2 is not totally chemically inert. It can be converted to CO in the high-temperature part of the flame. A check of the production rates for the relevant reactions involving CO and CO_2 shows that the conversion of CO_2 to CO is mainly due to the reaction $CO_2 + H \rightarrow CO + OH$. This

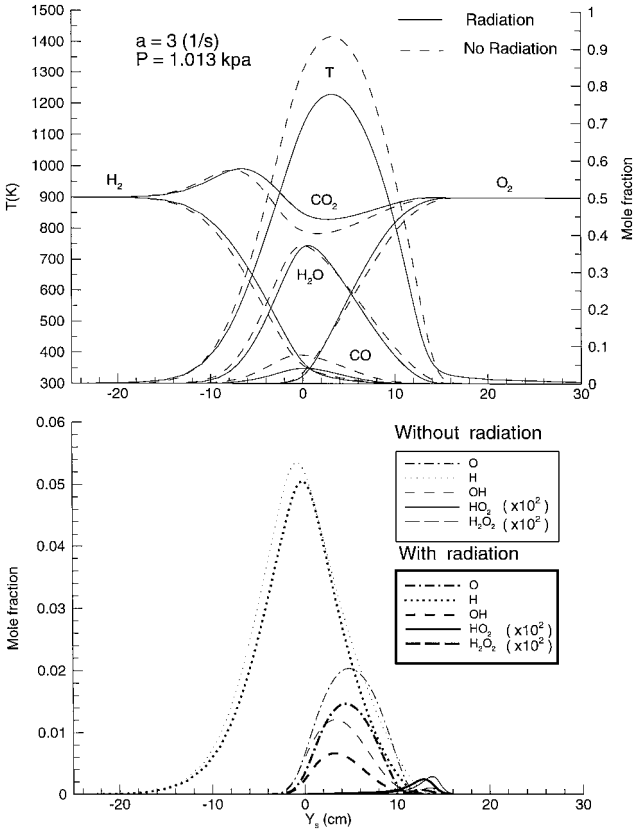

Fig. 4 Flame structure at $a = 3\ s^{-1}$ and 50% CO_2 dilution, with and without consideration of flame radiation.

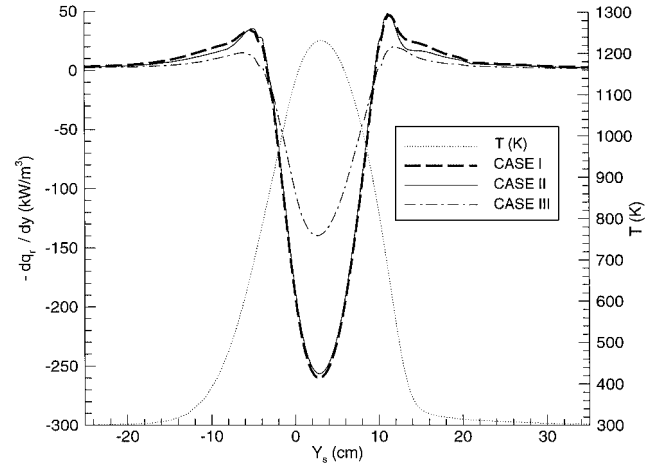

Fig. 5 Divergence of radiative heat flux based on the flame profile at $a = 3\ s^{-1}$, 50% CO_2 dilution.

behavior also was found in Ref. 27, but for different conditions. The roles of CO_2 are not limited to radiation and dilution, but also include some degree of chemical participation.

One of the unusual findings in the calculation is the existence of very thick diffusion flames. The diffusion flame thickness is of the order $(D/a)^{1/2}$, where D is the mixture diffusion coefficient. Because D is inversely proportional to pressure, P, the thickness is proportional to $(Pa)^{-1/2}$. Both low stretch and low pressure promote a thick diffusion flame. To be able to use the one-dimensional flame approximation in an experiment, one will need to have a flame with width-to-thickness ratio much greater than unity. If the flame is to be generated using two opposing nozzles, a large nozzle diameter, much larger than the flame thickness, is needed. Although this setup would be unusually large scale, it is feasible. If, in an experiment, the flame width-to-thickness ratio is not big enough, lateral heat conduction will exist at the flame edges, which clearly requires a multidimensional flame model.[28,29] On the other hand, since the extinction of low-stretch flames is by heat losses, the existence of this additional lateral heat conductive loss will render the flame less flammable than the corresponding case of a flame with large width-to-thickness ratio (which has only radiative loss). Thus, the computed one-dimensional case provides an upper limit in terms of flammability, which is useful from the point of view of fire safety. In addition, these thick low-stretch and low-pressure flames can be good candidates for experimental flame structure studies because good spatial resolution can be obtained rather easily.

Radiation Treatment

In the preceding section, it was mentioned that, at low pressures, collision broadening decreases and Doppler broadening becomes more important. In this section, the importance of collision and Doppler broadening is investigated by performing several radiation calculations using the calculated flame profile (as seen in Fig. 4) at $3\ s^{-1}$ and 50% CO_2 dilution. The radiative source profiles are shown in Fig. 5 for the three different cases: case 1, combined Doppler and collision broadening; case 2, only Doppler broadening; and case 3, only collision broadening. The negative values of the radiative source term correspond to net emission of radiative energy, whereas positive values correspond to net absorption of radiative energy. Case 1 shows that there is a net emission of radiative energy in the high-temperature part of the flame and net absorption at the edges, where the temperature is lower. Comparing this case with case 2 reveals that the Doppler broadening is dominant, especially at the high-temperature part of the flame, and there the two profiles are similar. On the other hand, a comparison between case 1 and case 3 shows that the collision broadening alone does not give an accurate prediction in the high-temperature region of the flame. Consequently, Doppler broadening has to be considered besides collision broadening in the radiation model at sufficiently low pressure. If an optically thin radiation model is used, the net radiation emission

will be overestimated and the absorption (mostly self-absorption) is neglected.[9,11]

Conclusions

In this numerical work, the one-dimensional diffusion flame of H_2 and O_2 have been solved with CO_2 as diluent. By coupling a narrowband radiation model with the OPPDIF program, a computation tool is made available to study the flame behavior and to explore the flammability limits with improved accuracy, especially at low flame stretch rates.

In the computations presented, the pressure chosen is 1.013 kPa (approximately the Martian atmospheric pressure). The upstream temperatures are 300 K on both the fuel and the oxygen sides. The CO_2 dilution levels are equal on both the fuel and the oxygen sides and are treated as a parameter in the computation together with the flame stretch rate.

Unlike the adiabatic theory, one-dimensional diffusion flame with radiation predicts the existence of an absolute CO_2 dilution limit. Above this limit, a diffusion flame cannot exist at any stretch rate. Below this absolute limit, there is an upper and a lower bound of flammable stretch rate. At 1.013 kPa, with more than 50% CO_2 dilution, the hydrogen–oxygen diffusion flame can be sustained only at stretch rates lower than 40 s^{-1}. This behavior is due to the slow chemical reactions at such a low-pressure level. The peak temperatures of these flames are quite low, much less than the adiabatic values. The decrease of flame temperature is the combined result of limited gas residence time (flame stretch) and radiative loss. In the flammability map presented, the domain where the effect of flame stretch dominates and the domain where the effect of flame radiation dominates are indicated.

Although the qualitative trends shown in this work are believed to be correct, the accuracy of the quantitative results will depend on the data used. Clearly, if these data are refined in the future, improved flame prediction can result. It is also of interest to test the predicted results experimentally, although a large-scale setup, a low-pressure facility, and probably a low-gravity environment will be needed.

Acknowledgments

This work is supported by NASA grant NAG3-1046. We would also like to thank Edward White and Franco Frate for their assistance.

References

[1]Pellett, G. L., Isaac, K. M., Humphreys, W. M., Jr., Gartrell, L. R., Roberts, W. L., Dancey, C. L., and Northam, G. B., "Velocity and Thermal Structure, and Strain-Induced Extinction of 14 to 100% Hydrogen-Air Counterflow Diffusion Flames," *Combustion and Flame*, Vol. 112, March 1998, pp. 575–592.

[2]T'ien, J. S., and Bedir, H., "Radiative Extinction of Diffusion Flames—A Review," *Proceedings of the First Asia-Pacific Conference on Combustion*, Osaka, Japan, 1997, pp. 345–352.

[3]Ronney, P. D., "Understanding Combustion Processes Through Microgravity Research," Plenary Lecture, *Proceedings of the 27th International Symposium on Combustion*, The Combustion Inst., Pittsburgh, PA, 1998, pp. 2485–2506.

[4]T'ien, J. S., "Diffusion Flame Extinction at Small Stretch Rates: The Mechanism of Radiative Loss," *Combustion and Flame*, Vol. 65, July 1986, pp. 31–34.

[5]Rhatigan, J. K., Bedir, H., and T'ien, J. S., "Gas Phase Radiative Effects on the Burning and Extinction of a Solid Fuel," *Combustion and Flame*, Vol. 112, Jan. 1998, pp. 231–241.

[6]Bedir, H., and T'ien, J. S., "A Computational Study of Flame Radiation in PMMA Diffusion Flame Including Fuel Vapor Participation," *Proceedings of the 27th International Symposium on Combustion*, The Combustion Inst., Pittsburgh, PA, 1998, pp. 2821–2828.

[7]Chan, S. H., Yin, J. Q., and Shi, B. J., "Structure and Extinction of Methane-Air Flamelet with Radiation and Detailed Chemical Kinetic Mechanism," *Combustion and Flame*, Vol. 112, Feb. 1998, pp. 445–456.

[8]Maruta, K., Yoshida, M., Guo, H., Ju, Y., and Niioka, T., "Extinction of Low-Stretched Diffusion Flame in Microgravity," *Combustion and Flame*, Vol. 112, Jan. 1998, pp. 181–187.

[9]Daguse, T., Croonenbroek, J. C., Rolon, J. C., Darabina, N., and Soufiani, A., "Study of Radiative Effects on Laminar Counterflow $H_2/O_2/N_2$ Diffusion Flame," *Combustion and Flame*, Vol. 106, Aug. 1996, pp. 271–287.

[10]Olson, S. L., "Buoyant Low Stretch Stagnation Point Diffusion Flames Over a Solid Fuel," Ph.D. Dissertation, Dept. of Mechanical and Aerospace Engineering, Case Western Reserve Univ., Cleveland, OH, 1997.

[11]Bedir, H., T'ien, J. S., and Lee, H. S., "Comparison of Different Radiation Treatments for a One-Dimensional Diffusion Flame," *Combustion Theory and Modeling*, Vol. 1, Dec. 1997, pp. 395–404.

[12]Wu, M. S., Liu, J. B., and Ronney, P. D., "Numerical Simulation of Diluent Effects on Flame Balls," *Proceedings of the 27th International Symposium on Combustion*, The Combustion Inst., Pittsburgh, PA, 1998, pp. 2543–2550.

[13]Hoffman, S. J., and Kaplan, D. I. (eds.), *Human Exploration of Mars: The Reference Mission of the NASA Mars Exploration Study Team*, NASA SP6107, 1997.

[14]Dixon-Lewis, G., "Structure of Laminar Flames," *Proceedings of the 23rd International Symposium on Combustion*, The Combustion Inst., Pittsburgh, PA, 1990, pp. 305–324.

[15]Smooke, M. D., and Giovangigli, V., *Formulation of the Premixed and Non-premixed Test Problems*, Lecture Notes in Physics, Ser. 384, Springer–Verlag, New York, 1991, Chap. 1.

[16]Ludwig, C. B., Malkmus, M., Reardon, J. E., and Thomson, J. A. L., *Handbook of Infrared Radiation by Combustion Gases*, edited by R. Goulard and J. A. L. Thomson, NASA SP3080, 1973.

[17]Soufiani, A., and Taine, J., "High Temperature Gas Radiative Property Parameters of Statistical Narrowband Model for H_2O, CO_2, and CO and Correlated k Model for H_2O and CO_2," *International Journal of Heat Mass Transfer*, Vol. 40, March 1997, pp. 987–991.

[18]Godson, W. L., "The Evaluation of Infrared Radiative Fluxes Due to Atmospheric Water Vapor," *Quarterly Journal of the Royal Meteorological Society*, Vol. 79, 1953, pp. 367–379.

[19]Kim, T. K., Menart, J. A., and Lee, H. S., "Nongray Radiative Gas Analyses Using SN Discrete Ordinates Method," *Journal of Heat Transfer*, Vol. 113, Nov. 1991, pp. 946–952.

[20]Lutz, A. E., Kee, R. J., Grcar, J. F., and Rupley, F. M., "OPPDIF: A FORTRAN Program for Computing Opposed-Flow Diffusion Flames," Sandia Labs. TR SAND96-8243, June 1996.

[21]Kee, R. J., Rupley, F. M., and Miller, J. A., "Chemkin II: A FORTRAN Chemical Kinetics Package for the Analysis of Gas-Phase Chemical Kinetics," Sandia Labs., TR SAND89-8009, Sept. 1989.

[22]Kee, R. J., Dixon-Lewis, G., Warnatz, J., Coltrin, M. E., and Miller, J. A., "FORTRAN Computer Code Package for the Evaluation of Gas-Phase Multi-component Transport Properties," Sandia Labs., TR SAND86- 8246, Dec. 1986.

[23]Kim, T. J., Yetter, R. A., and Dryer, F. L., "New Results on Moist CO Oxidation: High Pressure, High Temperature Experiments and Comprehensive Kinetic Modeling," *Proceedings of the 25th International Symposium on Combustion*, The Combustion Inst., Pittsburgh, PA, 1994, pp. 759–766.

[24]Gutheil, E., and William, F. A., "A Numerical and Asymptotic Investigation of Structure of Hydrogen-Air Diffusion Flames at Pressure and Temperature of High Speed Combustion," *Proceedings of the 23rd International Symposium on Combustion*, The Combustion Inst., Pittsburgh, PA, 1990, pp. 513–521.

[25]Zhao, J., Isaac, K. M., and Pellett. G. L., "Global Characteristics and Structure of Hydrogen-Air Counterflow Diffusion Flames," *Journal of Propulsion and Power*, Vol. 12, No. 3, 1996, pp. 534–542.

[26]Lewis, B., and von Elbe, G., *Combustion, Flames and Explosions of Gases*, 3rd ed., Academic International Press, 1987.

[27]Masri, A. R., Dibble, R. W., and Barlow, R. S., "Chemical Kinetic Effects in Non-premixed Flames of H_2/CO_2 Fuel," *Combustion and Flame*, Vol. 91, Dec. 1992, pp. 285–309.

[28]Takagi, T., Yoshikawa, Y., Yoshida, K., Komiyama, M., and Kinoshita, S., "Studies on Strained Non-premixed Flames Affected by Flame Curvature and Preferential Diffusion," *Proceedings of the 26th International Symposium on Combustion*, The Combustion Inst., Pittsburgh, PA, 1996, pp. 1103–1110.

[29]Frouzakis, C. E., Lee, J., Tomboulides, A. G., and Boulouchos, K., "Two-Dimensional Direct Numerical Simulation of Opposed-Jet Hydrogen/Air Diffusion Flame," *Proceedings of the 27th International Symposium on Combustion*, The Combustion Inst., Pittsburgh, PA, 1998, pp. 571–577.